

Cite this: *Nanoscale*, 2012, **4**, 5673

www.rsc.org/nanoscale

PAPER

Metal-filled carbon nanotube based optical nanoantennas: bubbling, reshaping, and *in situ* characterization

Zheng Fan,^a Xinyong Tao,^b Xudong Cui,^c Xudong Fan,^d Xiaobin Zhang^e and Lixin Dong^{*a}

Received 14th April 2012, Accepted 4th July 2012

DOI: 10.1039/c2nr30892d

Controlled fabrication of metal nanospheres on nanotube tips for optical antennas is investigated experimentally. Resembling soap bubble blowing using a straw, the fabrication process is based on nanofluidic mass delivery at the attogram scale using metal-filled carbon nanotubes (m@CNTs). Two methods have been investigated including electron-beam-induced bubbling (EBIB) and electromigration-based bubbling (EMBB). EBIB involves the bombardment of an m@CNT with a high energy electron beam of a transmission electron microscope (TEM), with which the encapsulated metal is melted and flowed out from the nanotube, generating a metallic particle on a nanotube tip. In the case where the encapsulated materials inside the CNT have a higher melting point than what the beam energy can reach, EMBB is an optional process to apply. Experiments show that, under a low bias (2.0–2.5 V), nanoparticles can be formed on the nanotube tips. The final shape and crystallinity of the nanoparticles are determined by the cooling rate. Instant cooling occurs with a relatively large heat sink and causes the instant shaping of the solid deposit, which is typically similar to the shape of the molten state. With a smaller heat sink as a probe, it is possible to keep the deposit in a molten state. Instant cooling by separating the deposit from the probe can result in a perfect sphere. Surface and volume plasmons characterized with electron energy loss spectroscopy (EELS) prove that resonance occurs between a pair of as-fabricated spheres on the tip structures. Such spheres on pillars can serve as nano-optical antennas and will enable devices such as scanning near-field optical microscope (SNOM) probes, scanning anodes for field emitters, and single molecule detectors, which can find applications in bio-sensing, molecular detection, and high-resolution optical microscopy.

Introduction

Spherical nanostructures on pillars (tubes or wires) can function as optical antennas^{1–5} for apertureless scanning near-field optical microscopy (SNOM),^{6,7} laser trapping,^{8,9} or single molecule detection^{10,11} in nanophotonic systems and scanning anodes for field emitters¹² in vacuum nanoelectronic devices. A variety of techniques have been developed to fabricate metallic nanostructures on a cantilever tip or an optical fibre using inversed self-assembly grafting,¹³ wet-chemistry surface assembly,¹⁴ water-flow suction,¹⁵ photocatalytic deposition,¹⁶ and optical

trapping.¹⁷ However, the controlled attachment of individual nanoparticles on nanopillars has been shown infeasible.¹⁸

On the other hand, the hollow cavities of carbon nanotubes (CNTs) allow a variety of metals such as Au, Ag, Cu, Sn, Fe, Co, and Ni and their alloys to be encapsulated inside the core.^{19–23} Mimicking soap bubbles blowing from a straw, the encapsulated metal may be bubbled over the nanotube tip if they can be flowed out and dwelled on the tip. Previously investigated electron-beam-induced flowing and extruding^{24–26} and current-driven electromigration are possible to be applied. However, several challenges remain due to the specialty of sphere-on-pillar structure extruded materials or deposits that must be spherical and dwell on the tube tip. (1) Previous investigations demonstrated that the exposure of metal-filled carbon nanotubes (m@CNTs) under a highly intensive electron beam resulted in the expansion, melting and flowing of the encapsulated materials, and potential applications such as thermometers and extruders have been demonstrated.^{24–26} However, a further step to flow these materials out from the nanotube onto the orifice has not yet been investigated. (2) It has been understood that irradiation of nanotubes can cause large pressure build-up within the nanotube cores that can plastically deform, extrude, and break solid

^aDepartment of Electrical and Computer Engineering, Michigan State University, East Lansing, MI 48824, USA. E-mail: ldong@egr.msu.edu; Fax: +1 517 353 1980; Tel: +1 517 353 3918

^bCollege of Chemical Engineering and Materials Science, Zhejiang University of Technology, Hangzhou 310014, China

^cDepartment of Material Science and Technology, Research Center of Laser Fusion, China Academy of Engineering Physics, Mianyang, Sichuan 621900, China

^dCenter for Advance Microscopy, Michigan State University, East Lansing, MI 48824, USA

^eDepartment of Materials Science and Engineering, Zhejiang University, Hangzhou 310027, China

materials.²⁵ The effects of the pressure on molten metal are still unclear. (3) Mass melting, flowing, evaporation, and deposition based on electromigration have been realized inside a nanotube,²⁷ between nanotubes,²⁸ and from a nanotube to other objects.^{23,29} These have enabled new techniques³⁰ such as nanorobotic spot welding²⁹ and devices such as archival memories.²⁷ However, the shape control of the deposits was beyond the interest of these applications.

Based on these insights, here we show fabrication processes specifically designed for delivering and dwelling the encapsulated materials from m@CNTs onto their tips targeting on achieving controllable sizes and shapes. The processes are named nanobubbling and include electron-beam-induced bubbling (EBIB) and electromigration-based bubbling (EMBB). It can be understood that the sizes of the spheres will be determined by the mass flow rate and the time, and the maximum sizes are limited by the total mass encapsulated. The final shapes of the deposits will be influenced by the cooling speed. Instant cooling down will result in a similar shape as that in a molten state whereas a slower cooling rate will involve recrystallization. A solid sphere forming from a crystal prefers instant cooling from a molten sphere where surface tension dominates the recrystallization so that a ball with high sphericity can be formed. Hence, heat sink arrangement will be a key towards fine shaping of the spheres by controlling the cooling rate.

Fabrication of sphere-on-pillar nanostructures

1. Setup

Our experiments were performed in a transmission electron microscope (TEM, JEOL 2200FS) with a field emission gun. The samples we used included Sn- and Cu-filled CNTs. The Sn@CNTs were synthesized by using catalytic deposition of acetylene using SnO₂.²⁶ During the process, the catalysts were directly placed into the furnace and without the preheating and reduction process. The diameters of Sn@CNTs ranged from 20 to 80 nm. Sn cores are single crystalline with good crystallization. The Cu-tipped CNTs were synthesized using an alkali-doped Cu catalyst by a thermal CVD method,²¹ and their outer diameters were in a range of 40–80 nm. The single crystalline Cu nanoneedles were encapsulated in graphite walls approximately 4 to 6 nm thick at the tips of CNTs. A single-tilt TEM holder was used for EBIB, and a scanning tunnelling microscope built in a TEM holder (FM2000E, Nanofactory Instruments AB) was adopted for EMBB.

2. EBIB using Sn-filled CNTs

During the EBIB (Fig. 1(a)), the current density of the electron beam transmitting through the CNTs was adjusted by changing the focus, the magnification, the brightness and the incident area. The final shapes can be either spheres or particles with multiple facets, which are related to the heating and cooling processes. The sizes of the spheres on the tips are found to be related to the exposure time and the orifices of the nanotube. A series of time-resolved TEM images (Fig. 1(b)) show that the EBIB of a Sn@CNT occurs at a current density of 20 A cm⁻² with the magnification of $\times 300k$ and the irradiation area of 1.3×10^{-14} cm². The accelerating voltage of the electron beam is maintained

at 200 kV in all experiments. By increasing the current density, the local temperature increased due to the higher electron energy. Starting from an as-synthesized Sn-filled CNT, it can be seen that a nanosphere has been formed on the tip of the CNT due to the exposure to the electron beam. At $t = 720$ s (Fig. 1(b)), the inner molten metal first broke out from the nanotube. In our previous investigations, we have observed that the tin nanowire melted entirely in the CNTs when the current density reached 0.4 A cm⁻², and the expansion of the tin wire occurred at the same time.²⁶ The much higher current density needed here (20 A cm⁻²) is attributed to the bubbling of the molten metal. At the beginning of the process, polyhedral nanoparticles (Fig. 1(b), 1200 s) were formed. By increasing the temperature further, it is possible to convert polyhedral nanoparticles into spheres (Fig. 1(b), 2880 s).³¹ We attribute the bubbling and the shape conversion to the electron irradiation and the secondary effects, including the carbon shell contraction and the surface tension of the molten metal. The encapsulated materials were melted and then squeezed out by the carbon shells as spheres onto the tip of nanotubes. Applying an image processing method, we analyzed the mass of the sphere. The CNT has an external diameter of approximately 40 nm. The diameter of the final sphere is 54 nm, and the mass of the resulted sphere is 0.6 fg (femtograms) according to the density of tin (7.31 g cm⁻³).

It is found that the threshold current density for the sphere formation is 20 A cm⁻² with the exposure time of ~ 720 s. Experiments on several other CNTs showed that the threshold current density varies from 10 to 25 A cm⁻² related to their diameters (37–40 nm). The curves for the bubbling vs. the diameter of the sphere are depicted in Fig. 1(c). It can be found that the starting time for the flowing out is shortened with the increase of irradiation energy. The starting time shortens from 700 to 200 s for the current density from 10 to 25 A cm⁻², and the bubbling time varies from 1900 to 3360 s, respectively. These variations may be related to the internal temperature and pressure build-up.

According to the experiments, the EBIB process consists of two parts, *i.e.*, the melting of the inner metal and the shrinkage of the carbon shells. The melting was caused by the heating of the tin by the irradiation effects as revealed in previous works.²⁶ The contraction of the carbon shells having been observed (Fig. 1(b), 720 to 1440 s) is responsible for the squeezing out of the sphere from the nanotube shell. The contraction is caused by electron beam irradiation on CNTs, which may generate a large pressure within the nanotube cores that can deform and extrude the metals from the carbon shells.²⁵ Moreover, the final shape of the nanostructure on the tip was largely dependent on whether the encapsulated materials are sufficiently melted. Sufficiently melted materials result in a perfect sphere in the molten state and the shape can be retained if the cooling down occurs instantly. A gradual cooling down will allow the particle to recrystallize, generating a facet structure as the high resolution TEM image resolves (Fig. 1(d)). The cooling speed is mainly determined by the incident beam energy and the dissipation from the nanotubes. It is possible to remelt and reshape the particle by injecting more thermal energy provided it is within what the beam intensity can achieve. So, the full process of EBIB is as follows: the rupture of the carbon planes makes defects on the carbon shells, and then the bubbling occurs at these sites. The internal pressure build-up

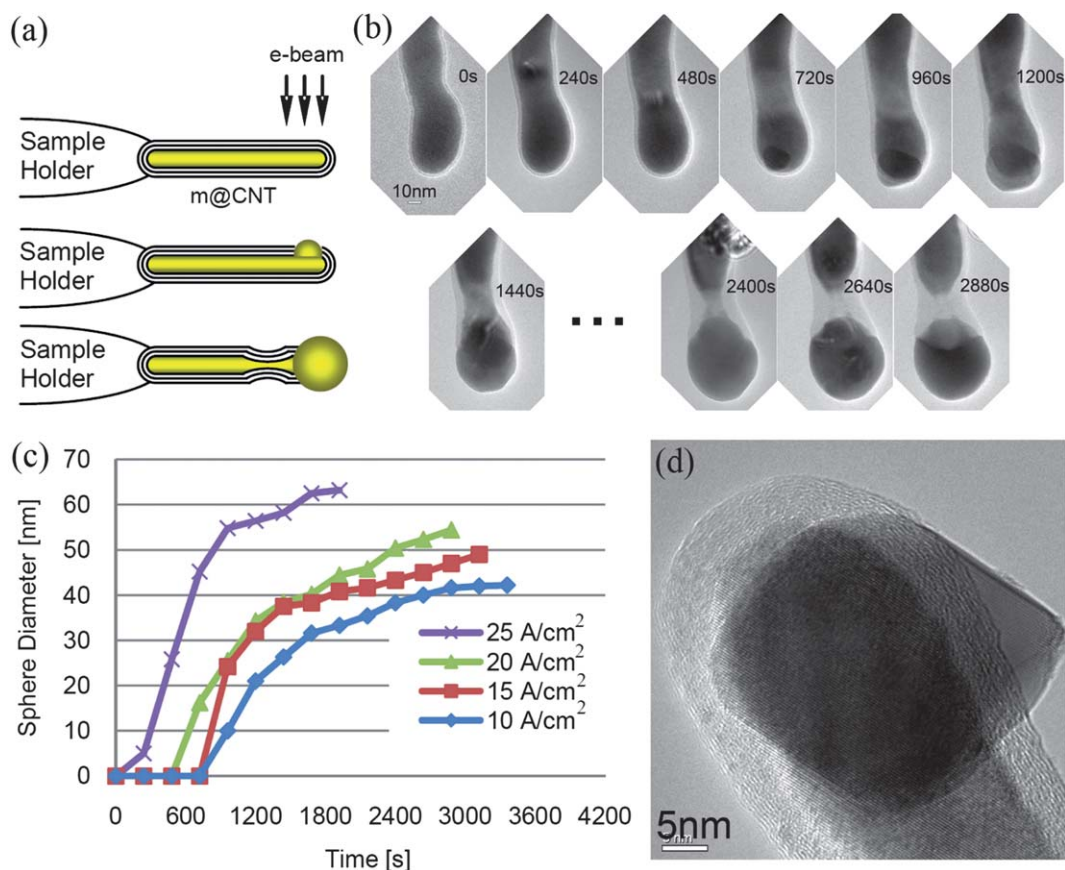


Fig. 1 (a) The schematic of EBIB. The inner metal of an m@CNT will melt and flow out of the carbon shell due to the exposure of the e-beam. (b) Time-resolved EBIB processes. A Sn@CNT was brought under the electron beam at $t = 0$ s. Under the current density of 20 A cm^{-2} from 240 to 480 s, a molten section of tin appeared and moved to the tip of the tube and the tube tip became more spherical. At $t = 720$ s, the inner metal first broke out from the tube. Then metal continued to flow out, and the carbon shell near the tip of the tube deformed severely, which may be responsible for the squeezing out of the sphere from the nanotube shell. At $t = 1440$ s, a sphere was visible on the tip of the CNT and at $t = 2880$ s, the sphere on the tip was complete, the shrinkage of the carbon shell prevented the metal flow from the bottom to the top of the tube. (c) Time sequences of bubbling differed at different current densities and tube sizes. (d) As the e-beam exposure suddenly stopped during EBIB, the squeezed-out metal recrystallized and resulted in a facet shape.

is a result of melting, the thermal expansion of the encapsulated metal, and the shrinkage of the nanotube shells,²⁵ which are all determined by the current density. As a result, the rates of the nanobubbling and the geometry of the spheres can be controlled by adjusting the current density.

3. EMBB using Cu-filled CNTs

The same EBIB procedures have been applied to Cu-filled CNTs, but bubbling did not occur at the highest possible current density. It implies that the e-beam from the TEM cannot reach the melting point of copper ($1083 \text{ }^\circ\text{C}$). As an alternative method, EMBB has been developed for Cu-filled CNTs. The setup of EMBB is depicted in Fig. 2(a). The FM2000E STM-TEM holder mentioned above is adopted for the experiments, in which a probe can be positioned in a millimeter-scale workspace with subnanometer resolution with the STM unit actuated by a three-degree-of-freedom piezotube, making it possible to select a specific CNT. Physical contact can be made between the probe and the tip of a nanotube. Applying a voltage between the probe and the sample holder establishes an electrical circuit through a

CNT and injects thermal energy into the system *via* Joule heating. By increasing the applied voltage, the local temperature can be increased and can pass the melting point of the copper encapsulated in a tube. Then, the encapsulated materials may be delivered from the carbon shells, and nanospheres are bubbled over the CNT tips. The EMBB process is similar to nanorobotic spot welding, but the focus is on the shape and size control of the deposited spots. During the experiments, the intensity of the electron beam has been maintained in the range for regular imaging, which is several orders of magnitude lower than the above-mentioned values for EBIB.

In the experiments, a Cu-filled CNT tip was first brought to contact with the STM probe, and then a bias voltage was applied on the two ends of the CNT. With the increase of the voltage from 0 V at a step of 0.1 V, the inner copper core flowed out to the tip of the CNT in a short time when it reached the range between 2.0 V and 2.5 V (Fig. 2(b)). The process was recorded by a real-time video, and the selected video frames of the melting process (Fig. 2(c)) reveal that a copper polyhedral nanoparticle was formed initially on the tip of the tube. Then, by increasing the bias further (the temperature and the driven force will be

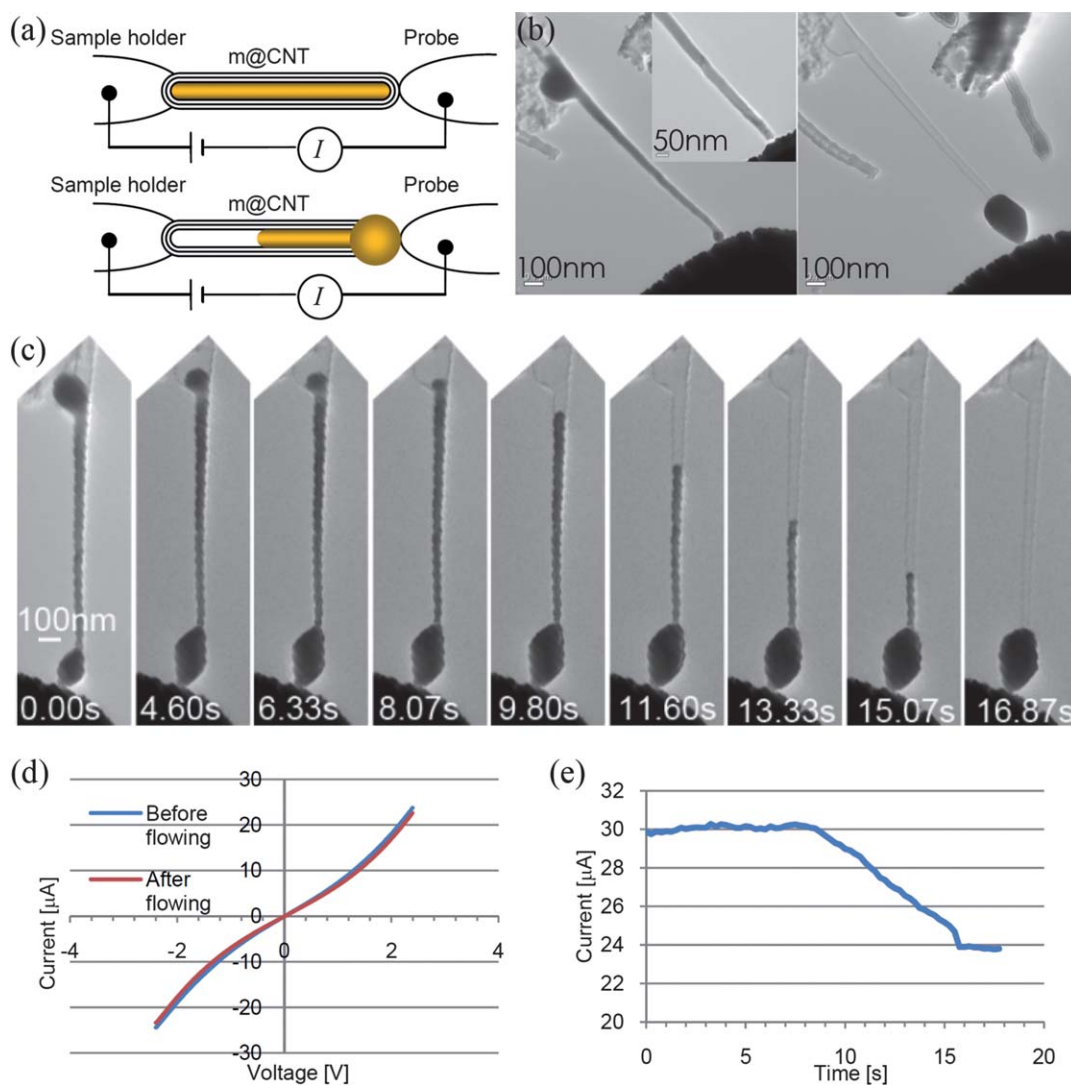


Fig. 2 (a) The schematic of EMBB. (b) A sphere on the tip formed by EMBB. (c) EMBB processes. The tip of the Cu@CNT was physically contacted with the probe. Applying a voltage between the probe and the sample holder establishes an electrical circuit through a CNT and injects thermal energy into the system *via* Joule heating. By increasing the applied voltage, the local temperature can be increased past the melting point of the copper encapsulated in a tube. Then, the encapsulated materials are delivered from the carbon shells, and nanospheres are bubbled over the CNT tips in a short time (16.87 s). (d) I - V characterization before and after the flowing. (e) I - t characterization during EMBB.

increased accordingly), a spherical particle formed on the tip of the nanotube. In this experiment, the flow out of the copper started at 2.4 V and the entire process continued for about 17 s. The flow rate was found to be 82.3 nm s^{-1} according to the length change of the inner copper core (Fig. 2(b)). The current vs. voltage (I - V) curves were obtained before and after the copper flowed out (Fig. 2(d)). It can be found by comparing the two I - V curves that the current through the CNT before flowing is larger than that after the flowing occurred. That is a result of the exposure of the carbon shells due to the loss of the encapsulated copper, which has better conductivity than the carbon shells. The current-time (I - t) curve simultaneously recorded by a multimeter (Fig. 2(e)) during the copper flowing out also showed that the current decreased along with the flowing time. Accordingly, the current density under the bias of 2.4 V dropped from $2.38 \times 10^6 \text{ A cm}^{-2}$ to $1.98 \times 10^6 \text{ A cm}^{-2}$; causing the cooling down of the deposit at the orifice. Moreover, heat dissipation increased

when more copper reached the probe. As the volume of the probe (tip radius: 70 nm, root radius: 10 μm) is absolutely larger than that of the copper deposit, the probe serves as a heat sink with essentially infinite capacity compared to the copper deposit. Hence, it was not possible to reheat the copper after cooling down. This can also explain why the flowed out materials crystallized immediately while the bias remained unchanged, and in most cases, without increasing the bias during the flowing, polyhedral nanoparticles will be formed. Similar to the role of heat sinks in electric breakdown of CNTs,^{32,33} the shape of the deposits is largely influenced by the thermal energy distribution and dissipation during the EMBB process. An enlarged image (Fig. 3(a)) of the same deposit as shown previously (Fig. 2(b)) illustrates that the large probe serves as a huge heat sink, which possesses excellent thermal conductivity to cool down the particle in a short time. The reheating or reshaping is unattainable due to the minimum distribution of thermal energy at the

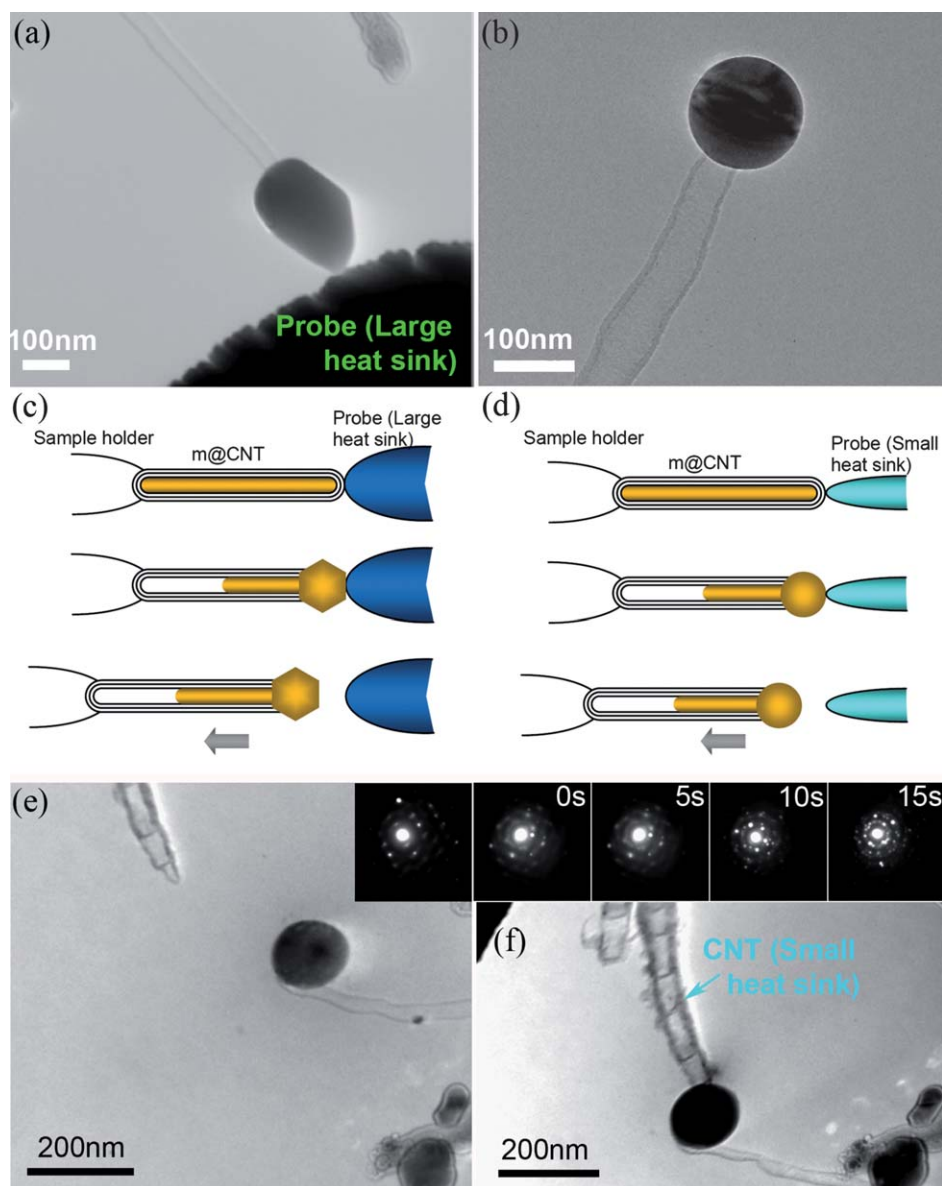


Fig. 3 The influence of heat sinks during EMBB processes. (a) The particle shows a facet shape as induced by a large probe, which has excellent thermal conductivity to cool down the particle in a short time. (b) The sphere on a nanotube induced by a small probe. The small size of the probe makes it possible to maintain thermal energy on the particle, which makes it remain in a molten state and shapes the particle into a perfect sphere. By separating the molten sphere from the probe, the spherical shape was retained. (c) The EMBB completed with a large probe served as a large heat sink. (d) The EMBB completed with a probe served as a small heat sink. (e) The sphere on a nanotube induced by a CNT which served as a small heat sink. The inset illustrates that the cool down sphere shows a single crystal diffraction pattern. (f) Reheating/remelting can be fulfilled by placing the sphere on the center of the CNT. Insets show the transformation of the sphere from a single crystal to a polycrystal, which represent the gradual melting process.

deposition site between the nanotube tip and the probe (heat sink). In contrast, if a small probe is applied, the spherical deposit can remain in the molten state and appears as spheres due to surface tension. A sudden cooling by separating the deposit from the biased probe can result in a perfect sphere (Fig. 3(b)). The influences of the volumes of heat sinks are schematically illustrated in parts (c) and (d) of Fig. 3. In the case of a large heat sink existence, the separation of the nanoparticle from the probe is not always achievable, *i.e.*, the nanotube will be soldered onto the probe. A CNT can serve as an ideal heat sink. Due to the similarity of the sizes to the m@CNT, the hottest spot can be positioned close to the contact point between the two CNT tips

where the bubble will be blown out. The probe CNT can also be used to reheat and reshape the nanoparticles obtained either from EBIB or EMBB (with a large heat sink). An example is shown in parts (e) and (f) of Fig. 3. A deposit was generated by EMBB under a bias of 2.4 V (Fig. 3(e)). The apparent shape of the deposit is spherical and the selected area electron diffraction (SAED) shows that the crystalline level is high although a perfect SAED pattern is unattainable due to the installation of the STM-TEM holder instead of a single-tilt one. By reattaching the probe CNT tip onto the sphere and increasing the bias from 1.0 V with a step of 0.2 V, melting occurs again as the voltage reaches up to 2.0 V. The particle starts to melt and the diffraction pattern

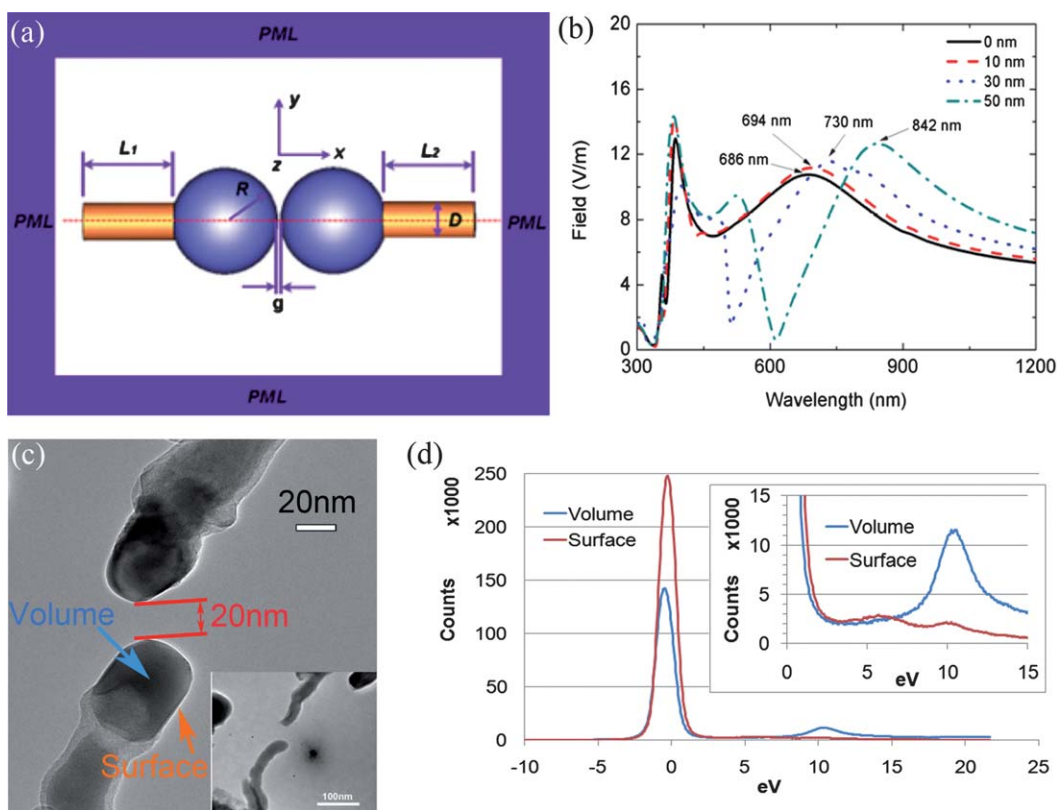


Fig. 4 (a) A model of a sphere-on-pillar optical nanoantenna. (b) Electric field strength in the center of the gap as a function of the wavelength for various CNT lengths. Some of the resonant wavelengths for the paired structures are indicated with corresponding arrows. (c) A pair of sphere-on-tip nanostructures fabricated by EBIB. Inset shows a pair of m@CNTs positioned together before EBIB is performed. (d) EELS excitation on the volume center and the surface of a sphere [refer to (c) for the positions that the electron beam focused on].

gradually changes (Fig. 3(f), inset). When the melting just started at 0 s, the diffraction pattern showed a highly crystallized phase. Along with the thermal energy being continuously injected into the particle, the crystal phase gradually transformed into more polycrystalline phases at 5, 10, and 15 s.

In situ characterization

As was proposed in our previous numerical studies, a pair of such sphere-on-pillar nanostructures (Fig. 4(a)) can function as optical antennas.³ In the numerical investigation, a metallic sphere that is attached at the near end of the nanotube has been mirrored accordingly to form a paired nanostructure ($L_1 = L_2$) with a feed gap. The feed gap g is initially selected to be 20 nm. The resulting computed spectral responses of the electric field in the center of the gap (antenna feed) for different nanotube lengths³ are illustrated (Fig. 4(b)). It is known that for plasmonic structures the surface plasmon (SP) resonances strongly depend on the shape and size of the structure as well as the losses from the materials.³⁴ To justify that the as-fabricated sphere-on-pillar pairs can function as optical antennas, experiments have been done using the STM-TEM holder in the same TEM. Two nanotubes are positioned close (Fig. 4(a), inset) and spheres are blown out from them using EBIB. Then, the two spheres are positioned close with a feed gap of 20 nm (Fig. 4(c)). The electron energy loss spectroscopy (EELS) technique is applied for *in situ* characterization of the resonance performance. The output

counts vs. excitation energy (in eV) curves are drawn (Fig. 4(d)). It can be seen that the volume plasmon (VP) appears at around 11 eV when the electron probe is placed at the center of the sphere. As the electron probe is placed close to the surface of a sphere, the surface plasmon peak becomes dominant around 6 eV (Fig. 4(d), the inset shows the details between 0 and 15 eV). These energy values correspond to the equivalent photons with wavelengths of 113 nm and 226 nm. It is evident that the surface plasmon has a lower energy and thus a larger wavelength, proving that resonance did occur.

Conclusions

In summary, we have proposed EBIB and EMBB for the controlled fabrication of sphere-on-pillar optical nanoantennas. Melting and bubbling of tin from nanotube shells have been realized at the current density of 10 to 25 A cm⁻². Bubbling started after the Sn@CNTs were exposed under the electron beam for 1900 to 3360 s based on their sizes. The melting of the encapsulated tin is the result of the carbon displacement threshold energy reached by the beam irradiation, which is also the reason for the destruction of carbon shells. The beam irradiation caused internal pressure build-up that is attributed to the melting and thermal expansion of the encapsulated materials and the shrinkage of the nanotube shells, which finally pushed out the molten metal and formed bubbles. It is necessary to contact the nanotube to electrode in EBIB technique. A better application

can be found in encapsulated materials with a low melting point. For the materials with a high melting point, EMBB is an alternative method to use. By applying a bias voltage as low as 2.0–2.5 V, the bubbling has been realized from Cu-filled CNTs. The Cu-filled CNT in the experiment has a 40-nm diameter, and the flow continued for 17 s at the flow rate of 82.3 nm s⁻¹. The bias threshold for the flowing was 2.4 V. Due to the contact between the CNT tip and a counterelectrode, new challenges raised in the process. The heat sinking into the electrodes may cause the immediate cooling down and recrystallization of the deposits during the draining of the CNT. Therefore, another nanotube was used in the experiment as a thermal resistive surface to retain the molten deposit in a spherical shape. By separating the deposit and the probe nanotube suddenly, the shape can be retained. This process can also be used for remelting and reshaping as-fabricated particles on nanotubes from EBIB and EMBB with a large heat sink. The volume and surface plasmon resonances have been tested using the EELS technique; proving that resonance did occur in this structure. Experimentally, this can be achieved more readily than near-field optical methods.

Sphere-on-tip architectures added a new design to the family of optical nanoantennas. With a combination of the proposed fabrication processes to directed growth of metal-filled nanotube arrays, batch fabrication of such devices is possible whereas the single devices can already be used as SNOM probes, single molecule detectors, and solar cell antennas to enhance their energy conversion. Furthermore, photonic crystals based on sphere-on-pillar arrays can be enabled. CNTs have a melting point (~3000 K in the vacuum) higher than almost any known material except for tungsten, so the process can be universally applied to all important materials for nanophotonics.

Acknowledgements

This work is supported by the NSF (IIS-1054585), the NSFC (51002138), the Zhejiang Provincial NSF of China (Y4090420), the Qianjiang Talent Project (2010R10029), the 'Qianjiang Scholars' program and the project sponsored by SRF for ROCS (2010609), SEM.

References

- 1 L. Novotny, *Nature*, 2008, **455**, 887.
- 2 P. Muhlschlegel, H. J. Eisler, O. J. F. Martin, B. Hecht and D. W. Pohl, *Science*, 2005, **308**, 1607–1609.
- 3 X. D. Cui, L. X. Dong, W. H. Zhang, W. Wu, Y. Tang and D. Erni, *Appl. Phys. B: Lasers Opt.*, 2010, **101**, 601–609.
- 4 A. M. Kern and O. J. F. Martin, *Nano Lett.*, 2011, **11**, 482–487.
- 5 P. Bharadwaj and L. Novotny, *Nano Lett.*, 2011, **11**, 2137–2141.
- 6 T. Kalkbrenner, U. Hakanson, A. Schadle, S. Burger, C. Henkel and V. Sandoghdar, *Phys. Rev. Lett.*, 2005, **95**, 200801.
- 7 M. Fleischer, A. Weber-Bargioni, M. V. P. Altoe, A. M. Schwartzberg, P. J. Schuck, S. Cabrini and D. P. Kern, *ACS Nano*, 2011, **5**, 2570–2579.
- 8 M. Righini, P. Ghenuche, S. Cherukulappurath, V. Myroshnychenko, F. J. G. de Abajo and R. Quidant, *Nano Lett.*, 2009, **9**, 3387–3391.
- 9 M. L. Juan, M. Righini and R. Quidant, *Nat. Photonics*, 2011, **5**, 349–356.
- 10 P. Anger, P. Bharadwaj and L. Novotny, *Phys. Rev. Lett.*, 2006, **96**, 113002.
- 11 C. Hoppe and L. Novotny, *Nano Lett.*, 2008, **8**, 642–646.
- 12 L. X. Dong, A. Subramanian, D. Hugentobler, B. J. Nelson and Y. Sun, *Adv. Rob.*, 2006, **20**, 1281–1301.
- 13 O. Sqalli, M. P. Bernal, P. Hoffmann and F. Marquis-Weible, *Appl. Phys. Lett.*, 2000, **76**, 2134–2136.
- 14 I. U. Vakarelski and K. Higashitani, *Langmuir*, 2006, **22**, 2931–2934.
- 15 Y. Kawata, S. Urahama, M. Murakami and F. Iwata, *Appl. Phys. Lett.*, 2003, **82**, 1598–1600.
- 16 T. Okamoto and I. Yamaguchi, *J. Microsc.*, 2001, **202**, 100–103.
- 17 F. Pampaloni, G. Lattanzi, A. Jonas, T. Surrey, E. Frey and E. L. Florin, *Proc. Natl. Acad. Sci. U. S. A.*, 2006, **103**, 10248–10253.
- 18 Y. Gan, *Rev. Sci. Instrum.*, 2007, **78**, 081101.
- 19 A. Chu, J. Cook, R. J. R. Heesom, J. L. Hutchison, M. L. H. Green and J. Sloan, *Chem. Mater.*, 1996, **8**, 2751–2754.
- 20 D. Ugarte, A. Chatelain and W. A. de Heer, *Science*, 1996, **274**, 1897–1899.
- 21 X. Y. Tao, X. B. Zhang, J. P. Cheng, Z. Q. Luo, S. M. Zhou and F. Liu, *Diamond Relat. Mater.*, 2006, **15**, 1271–1275.
- 22 P. M. Ajayan, T. W. Ebbesen, T. Ichihashi, S. Iijima, K. Tanigaki and H. Hiura, *Nature*, 1993, **362**, 522–525.
- 23 K. Svensson, H. Olin and E. Olsson, *Phys. Rev. Lett.*, 2004, **93**, 145901.
- 24 Y. H. Gao and Y. Bando, *Nature*, 2002, **415**, 599.
- 25 L. Sun, F. Banhart, A. V. Krashenninnikov, J. A. Rodriguez-Manzo, M. Terrones and P. M. Ajayan, *Science*, 2006, **312**, 1199–1202.
- 26 X. Y. Tao, L. X. Dong, W. K. Zhang, X. B. Zhang, J. P. Cheng, H. Huang and Y. P. Gan, *Carbon*, 2009, **47**, 3122–3127.
- 27 G. E. Begtrup, W. Gannett, T. D. Yuzvinsky, V. H. Crespi and A. Zettl, *Nano Lett.*, 2009, **9**, 1835–1838.
- 28 L. X. Dong, X. Y. Tao, M. Hamdi, L. Zhang, X. B. Zhang, A. Ferreira and B. J. Nelson, *Nano Lett.*, 2009, **9**, 210–214.
- 29 L. X. Dong, X. Y. Tao, L. Zhang, X. B. Zhang and B. J. Nelson, *Nano Lett.*, 2007, **7**, 58–63.
- 30 L. X. Dong, X. Y. Tao, L. Zhang, X. B. Zhang and B. J. Nelson, *IEEE Nanotechnol. Mag.*, 2010, **4**, 13–22.
- 31 X. D. Feng, D. C. Sayle, Z. L. Wang, M. S. Paras, B. Santora, A. C. Sutorik, T. X. T. Sayle, Y. Yang, Y. Ding, X. D. Wang and Y. S. Her, *Science*, 2006, **312**, 1504–1508.
- 32 J. Y. Huang, S. Chen, S. H. Jo, Z. Wang, D. X. Han, G. Chen, M. S. Dresselhaus and Z. F. Ren, *Phys. Rev. Lett.*, 2005, **94**, 236802.
- 33 X. Y. Huang, Z. Y. Zhang, Y. Liu and L. M. Peng, *Appl. Phys. Lett.*, 2009, **95**, 143109.
- 34 J. Rybczynski, K. Kempa, Y. Wang, Z. F. Ren, J. B. Carlson, B. R. Kimball and G. Benham, *Appl. Phys. Lett.*, 2006, **88**, 203122.